AMERICAN JOURNAL OF PHYSIOLOGY
RENAL PHYSIOLOGY

Am J Physiol Renal Physiol 325: F271–F282, 2023.
First published July 13, 2023; doi:10.1152/ajprenal.00083.2023

RESEARCH ARTICLE

N-acetylcysteine treatment attenuates hemodialysis access-related limb pathophysiology in mice with chronic kidney disease

Kyoungrae Kim,[2] Tomas A. Cort,[2] Eric M. Kunz,[2] Jack Moerschel,[2] Victoria R. Palzkill,[2] Gengfu Dong,[2] Chatick N. Moparthy,[2] Erik M. Anderson,[1,4] Brian Fazzone,[1,4] Kerri A. O'Malley,[1,4] Scott T. Robinson,[1,4] Scott A. Berceli,[1,4] Terence E. Ryan,[2,3] and Salvatore T. Scali[1,4]

[1]*Division of Vascular Surgery and Endovascular Therapy, University of Florida, Gainesville, Florida, United States;* [2]*Department of Applied Physiology and Kinesiology, University of Florida, Gainesville, Florida, United States;* [3]*Center for Exercise Science, University of Florida, Gainesville, Florida, United States; and* [4]*Malcom Randall Veteran Affairs Medical Center, University of Florida, Gainesville, Florida, United States*

Abstract

The objective of the present study was to determine if treatment with *N*-acetylcysteine (NAC) could reduce access-related limb dysfunction in mice. Male and female C57BL6J mice were fed an adenine-supplemented diet to induce chronic kidney disease (CKD) prior to the surgical creation of an arteriovenous fistula (AVF) in the iliac vascular bundle. AVF creation significantly increased peak aortic and infrarenal vena cava blood flow velocities, but NAC treatment had no significant impact, indicating that fistula maturation was not impacted by NAC treatment. Hindlimb muscle and paw perfusion recovery and muscle capillary density in the AVF limb were unaffected by NAC treatment. However, NAC treatment significantly increased the mass of the tibialis anterior ($P = 0.0120$) and soleus ($P = 0.0452$) muscles post-AVF. There was a significant main effect of NAC treatment on hindlimb grip strength at *postoperative day 12* (*POD 12*) ($P = 0.0003$), driven by significantly higher grip strength in both male ($P = 0.0273$) and female ($P = 0.0031$) mice treated with NAC. There was also a significant main effect of NAC treatment on the walking speed at *postoperative day 12* ($P = 0.0447$), and post hoc testing revealed an improvement in NAC-treated male mice ($P = 0.0091$). The area of postsynaptic acetylcholine receptors ($P = 0.0263$) and motor endplates ($P = 0.0240$) was also increased by NAC treatment. Interestingly, hindlimb skeletal muscle mitochondrial oxidative phosphorylation trended higher in NAC-treated female mice but was not statistically significant ($P = 0.0973$). Muscle glutathione levels and redox status were not significantly impacted by NAC treatment in either sex. In summary, NAC treatment attenuated some aspects of neuromotor pathology in mice with chronic kidney disease following AVF creation.

NEW & NOTEWORTHY Hemodialysis via autogenous arteriovenous fistula (AVF) is the preferred first-line modality for renal replacement therapy in patients with end-stage kidney disease. However, patients undergoing AVF surgery frequently experience a spectrum of hand disability symptoms postsurgery including weakness and neuromotor dysfunction. Unfortunately, no treatment is currently available to prevent or mitigate these symptoms. Here, we provide evidence that daily *N*-acetylcysteine supplementation can attenuate some aspects of limb neuromotor function in a preclinical mouse model of AVF.

arteriovenous fistula; dialysis; end-stage kidney disease; mitochondria; N-acetylcysteine

INTRODUCTION

For patients with end-stage kidney disease (ESKD), hemodialysis is the most common renal replacement therapy that is used to remove waste products from the blood, making it an indispensable life-sustaining treatment in this population. A well-functioning vascular access remains a critical barrier for patients with ESKD that require chronic hemodialysis. Several options are available for establishing permanent vascular access including central venous catheters as well as different configurations of arteriovenous graft and autogenous arteriovenous fistula (AVF) (1). Among these choices, AVFs are the most commonly used access due to their overall superior performance and durability. Although a high-quality, reliable AVF is preferred in many scenarios, it can be associated with a spectrum of postoperative hand and limb disabilities in 30–60% of patients, which is commonly referred to by the misnomer "steal syndrome" (2). Hand disability symptoms can range from subtle alterations in sensation to motor impairment causing weakness and, in rare cases, digital ulceration with or without gangrene. Historically, the cause of access-related hand dysfunction (ARHD) was believed to be primarily driven by hemodynamic perturbations following AVF creation; however, analysis of a well-characterized patient

Correspondence: S. T. Scali (salvatore.scali@surgery.ufl.edu).
Submitted 3 April 2023 / Revised 20 June 2023 / Accepted 5 July 2023

cohort found that hemodynamic alterations correlated poorly with the degree of hand disability, indicating that other factors likely contribute to ARHD (2).

There is a wealth of literature documenting that the systemic milieu of chronic kidney disease (CKD) has profound negative consequences on skeletal muscle (3–6), resulting in atrophy and muscle weakness that further promote a sedentary lifestyle. Elevated levels of oxidative stress and impaired mitochondrial function have emerged as potential drivers of muscle impairment in CKD (5–13). Notably, both oxidative stress and mitochondrial health represent growing areas of therapeutic development (14–17), yet their role in the development of ARHD following AVF creation has been largely unexplored. In the present study, we tested the hypothesis that treatment with *N*-acetylcysteine (NAC), a glutathione precursor with a strong safety profile, would ameliorate limb dysfunction in a recently developed murine iliac AVF model (18, 19).

METHODS

Animals and CKD Induction

Male and female C57BL/6J mice at 8–10 wk old were purchased from Jackson Laboratory. After arriving at the housing facility, animals underwent environmental acclimation (~50% humidity, 12:12-h light-dark cycle, ~22°C) and a diet transition phase from normal chow to 20% casein-based chow for 7 days, respectively. Thereafter, mice were fed a 0.2% adenine-supplemented casein chow diet to induce and maintain renal dysfunction. All animals were fed ad libitum for the duration of the experiment. To confirm renal insufficiency, whole blood was collected in heparinized capillary tubes via a tail snip, plasma was separated via centrifugation at 4,000 rpm for 10 min (4°C), and the blood urea nitrogen level was measured using a commercial kit (K024, Arbor Assays). All animal experiments adhered to the National Institutes of Health Guide for the Care and Use of Laboratory Animals and any updates. The Institutional Animal Care and Use Committee of the University of Florida and Malcom Randall Veterans Affairs Medical Center approved all procedures.

NAC Intervention

Animals were randomized to either the treatment group, which received NAC (150 mg/kg dissolved in 0.1 mL of 0.9% saline, adjusted pH ~7), or the control group, which received 0.9% saline (20, 21). Both treatments were delivered via oral gavage daily beginning 3 days before the AVF surgery with the final treatment occurring the day before euthanasia. To minimize animal stress during the gavage process, each animal underwent several familiarization sessions before the first intervention, and oral gavage was carried out by experienced technicians during the dark cycle using reusable metal gavage needles (20-gauge × 38 mm). After the oral gavage intervention, mice were carefully monitored for normal behavior retention and returned to their original cage rack. We chose the oral gavage approach because NAC has a strong sulfuric odor and unpleasant taste, which can lead to a reluctance of drinking, dehydration, and increased variance in dosage across animals.

Animal Model of Hemodialysis Access-Related Hand Dysfunction

After 2 wk of 0.2% adenine diet consumption, animals underwent surgery to create an iliac AVF as previously described (18, 19, 22). After initial isoflurane anesthesia, buprenorphine HCl (0.1 mg/kg) was administered subcutaneously, mice were placed on the surgical plate in a supine position, and abdominal hair was removed using a pen trimer. The surgical field was then disinfected with alternating chlorhexidine and alcohol wipes. A midline laparotomy from the pubis symphysis to the sternal margin was made and maintained with retractors. Next, intraperitoneal components including the small and large bowels, seminal vesicles, uterine horns, and ureters were gently moved and covered by a saline-soaked nonwoven sponge to secure exposure of the surgical window and explore the target vessels. Heparinized saline (0.2 IU/g) was injected via the inferior vena cava to prevent systemic coagulation and improve AVF patency outcomes. Small vessel branches, which can cause potential bleeding issues, were ligated using low-temperature cautery, and the left common iliac artery and vein were carefully dissected from the underlying retroperitoneal musculature using straight and angled forceps. Two 4-0 silk sutures were placed at the proximal and distal ends of the iliac artery-iliac vein bundle and used to vessel loop control the arteriovenous vasculature. Following the longitudinal venotomy (~1 mm), a 10-0 nylon imbricating suture was used to gently displace the posterior iliac vein and juxtaposed anterior iliac artery wall. Once this was completed, an ~0.8–9 × 0.3-mm elliptical incision was made into the conjoined poster iliac vein/anterior iliac artery wall to establish the fistula connection using Vannas spring scissors, followed by a 0.9% saline wash. Next, the anterior wall venotomy incision was repaired using two to three interrupted 10-0 nylon sutures followed by placement of the vascular bundle into its normal anatomic position. Subsequently, the two 4-0 silk suture vessel loops were loosened carefully and the site of the arteriovenous anastomosis as well as the surrounding tissues were gently blotted by saline-soaked pointed cotton swabs to restore blood flow. After AVF patency was confirmed by visualization of pulsatile, bright red oxygenated blood entering the iliac vein and mixing with dark venous blood returning from the hindlimb, the midline celiotomy incision was closed. Before the mouse was returned to the recovery cage, to further verify the presence of AVF steal-mediated hypoperfusion, blood perfusion within the tibialis anterior (TA) and ventral paw was measured using laser-Doppler flowmetry (moorVMS-LDF, Moor Instruments). Mice were provided moisturized food in a prewarmed recovery cage for 48 h postoperatively. Daily monitoring was performed postoperatively, and additional saline and/or buprenorphine were given as needed. Animals with deteriorating conditions or excessive tissue necrosis were euthanized.

Assessment of Fistula Patency and Systemic Hemodynamics

High-resolution digital images of the arteriovenous anatomy, including the infrarenal aorta and inferior vena cava, were captured using a high-frequency duplex ultrasound

system (30–50 MHz, Vevo 2100, VisualSonics, Toronto, ON, Canada) 2–3 days before the AVF creation and on *postoperative days* (*PODs*) *3* and *13*. These longitudinal hemodynamic assessments confirmed fistula patency and characterized central hemodynamic changes. After the induction of general anesthesia via isoflurane, mice were placed on a prewarmed three-dimensional positioning platform in a supine position and extremities were fixed with tape. AVF patency was ascertained using color and pulse-wave Doppler ultrasound where the increased peak systolic velocity with mixed arteriovenous blood flow existed in the juxta-anastomotic position. In addition, images surrounding the AVF anastomosis as well as within the distal aorta and cephalad portion of the inferior vena cava were obtained. Next, the diameter and peak systolic velocity of the infrarenal aorta and inferior vena cava were assessed using B-mode imaging and pulse-wave Doppler ultrasound at an insonation angle of 60°.

Hindlimb Perfusion Recovery Assessment

Postoperative blood perfusion to the hindlimb was measured using a laser-Doppler flowmeter (moorVMS-LDF, Moor Instruments) immediately after the AVF surgery and on *postoperative days 3* and *13* as previously described (19). Both hindlimbs were shaved, and the laser-Doppler probe was placed ~1–2 mm away from the middle belly of the TA and the middle of the posterior side of the paw. The perfusion was measured for ~10 s, and average perfusion was calculated. Perfusion recovery was calculated as a percentage of the AVF limb (left limb) relative to the contralateral nonsurgical limb (right limb).

Treadmill Walking Performance

Prior to the AVF surgery, each mouse underwent a familiarization protocol to establish baseline walking test performance on a speed-adjustable treadmill belt covered by a transparent box container (DigiGait, Mouse Specifics, Framingham, MA) at a speed of 5–10 cm/s up to 20 cm/s. Postoperatively, treadmill testing was performed 4 and 12 days after the AVF surgery. More specifically, each mouse was placed on the treadmill belt and started walking at the initial speed of 5 cm/s and the belt speed was gradually increased up to 20 cm/s. If the mouse hesitated to walk, acoustic motivation was provided by gentle tapping of the box container. Once the mouse was unable to maintain the next level of speed for a duration of 5–10 s despite additional stimulation, the maximal walking speed was recorded.

Grip Strength Test

Prior to the AVF surgery, each mouse underwent habituation training with exposure to unilateral hindlimb grip strength testing using a BIO-GS3 (BIOSEB) grip strength meter. Following the AVF formation, repeated unilateral hindlimb grip strength testing was performed on *postoperative days 4* and *12* to assess global limb changes in muscle strength. For this procedure, animals were gently held by the base of the tail and one hindlimb paw was allowed to firmly grasp the T-bar connected to the grip strength meter. Once the paw grip was secured, the mouse was gently pulled away from the T-bar and the peak force (in g) was recorded. The highest grip strength among 5–10 consecutive trials was used for analysis, and data were expressed as a percentage of the nonsurgical control limb.

In Situ EDL Muscle Function Testing

The contractile properties of the extensor digitorum longus (EDL) muscle were determined using the Aurora Scientific in situ muscle testing system. The testing platform was prewarmed via the water circulating system set at 38°C. Mice were anesthetized with an intraperitoneal injection of ketamine (90 mg/kg) and xylazine (10 mg/kg), and the mouse was positioned on the dissection board in the supine position. After hair removal, a small portion of skin on top of the foot was excised to expose the distal tendon of the TA and EDL muscles. A double square knot followed by a loop square knot was positioned immediately distal to the myotendinous junction of the tendon of the EDL muscle using a 4-0 silk suture. Subsequently, a double square knot using a 4-0 silk suture was positioned on the patella ligament. Thereafter, the animal was moved to the testing platform in the prone position and the knee and foot were secured to the testing platform using the patella ligament suture line and metal pins. Monopolar electromyogram needle electrodes were inserted next to the common peroneal nerve ~1 cm away from the fibula head. The distal EDL tendon was severed, and the suture was attached to the lever arm. Next, the optimum length was found using twitch stimulation at various lengths with 30-s intervals between stimuli, and contractile function was tested using a series of isometric contractions (1, 25, 50, 75, 100, 125, 150, and 175 Hz, 0.2-ms pulses for 300 ms) with 60-s intervals between stimuli (positive pulse phase and constant out pulse at 40 V).

Immunofluorescence Microscopy

Skeletal muscle cross-sectional area (CSA) and capillarization were evaluated using immunofluorescence microscopy as previously described (19). Following in situ EDL muscle functional testing, the TA and soleus muscles were excised, placed in disposable base molds with embedding medium compound, and frozen in liquid nitrogen-cooled 2-methylbutane. Three transverse sections (10 μm) of the TA and soleus were cut at the mid-belly using a Leica 3050S cryostat at −20°C, mounted on microscope slides, and stored at −20°C until immunofluorescence staining. Frozen muscle sections were briefly air-dried at room temperature and fixed with 4% paraformaldehyde for 5 min. Following multiple washes with 1× PBS, sections were permeabilized with 0.3% Triton X-100 in PBS for 10 min. After several washes with 1× PBS, sections were incubated in a blocking buffer (5% goat serum and 1% BSA in PBS) for 1 h. Thereafter, sections were incubated with primary antibody against laminin (Cat. No. L9393, Millipore-Sigma, 1:100 dilution) overnight at 4°C to label the sarcolemma. After multiple washes with 1× PBS, sections were stained with secondary antibody in blocking buffer (Alexa Fluor 488 goat anti-rabbit IgG, Cat. No. A-11008, Thermo Fisher Scientific, 1:250) along with Dylight 649-conjugated *Griffonia simplicifolia* lectin I isolectin B4 (Cat. No. DL-1208, Vector Laboratories) to stain capillaries. Coverslips were mounted with fluorescent mounting medium (Cat. No. H-1500, Vector Laboratories). Slides were imaged at ×20 magnification with an Evos FL2 Auto

microscope (Thermo Fisher Scientific). Myofiber CSA and capillary density were analyzed using MuscleJ (23).

Assessment of Postsynaptic Area Morphology

Once the in situ muscle functional test was completed, the EDL muscle was dissected from the AVF limb and placed in a Sylgard-covered petri dish filled with ice-cold PBS. After removal of visible blood and connective tissue endings, the EDL muscle bundle was gently teased using 45° angled forceps and bundles were treated with 3.2% paraformaldehyde for 10 min. After fixation, bundles were washed (3 × 5 min) in PBS and subsequently permeabilized in PBS supplemented with 2% Triton X-100 for 30 min with gentle shaking on a rocker at room temperature. Next, bundles were placed in blocking solution (1% Triton X-100 and 4% BSA in PBS) with mild shaking at 4°C overnight. After being blocked, muscle bundles were incubated with Alexa Fluor-488 conjugated α-bungarotoxin (Cat. No. B13422, Thermo Fisher Scientific) for 24 h to label postsynaptic acetylcholine receptor (AChR) clusters. On the next day, muscle bundles were washed again in PBS, mounted on a microscope slide with mounting medium (Cat. No. H-1500, Vector Laboratories), and then sealed with hard nail polish. Thereafter, slides were processed to acquire postsynaptic acetylcholine cluster images using a confocal microscope (Leica DMI 8) using the following acquisition parameters: objective, ×40; format, 1,024 × 1,024; speed, 600; bidirectional, ON; and *Z*-step size, 0.5 μm. Acquired images (46 ± 23.1 fibers) were quantified using the NMJ-morph semiautomatic macro tool in Fiji (24). Key determinants, such as AChRs, motor endplate, compactness (AChR area/endplate area × 100), and fragmentation (1 − 1/number of AChR clusters) were quantified. Investigators involved in the imaging and analysis process were blinded by the treatment conditions.

Isolation of Skeletal Muscle Mitochondria

Hindlimb skeletal muscle mitochondria were isolated as previously described (13, 25). The plantaris and gastrocnemius muscles were carefully dissected, cleaned off blood, fat, and connective tissues, and then minced with scissors on an ice-cooled petri dish. Thereafter, the minced muscle was incubated in ice-cold mitochondrial isolation media (MIM; 50 mM MOPS, 100 mM KCl, 1 mM EGTA, and 5 mM $MgSO_4$) containing 0.025% (wt/vol) trypsin for 3 min, followed by centrifugation at 800 *g* for 5 min at 4°C. The resulting supernatant containing trypsin was decanted, and the pellet was resuspended with ~12 mL MIM containing 0.02% (wt/vol) BSA (2 g/L). The sample was homogenized on ice using a glass-Teflon homogenizer and centrifuged at 800 *g* for 10 min at 4°C. The resulting supernatant was transferred into a new tube and centrifuged again at 10,000 *g* for 10 min at 4°C, resulting in a mitochondria-rich pellet. The pellet was washed with MIM (without BSA) to remove damaged mitochondria and the BSA included MIM at least twice and then gently resuspended in MIM (without BSA). The protein concentration of the resuspension was assessed using a bicinchoninic acid protein assay (Cat. No. A53225, Thermo Fisher Scientific).

Assessment of Mitochondrial Function

A high-resolution respirometry Oxygraph-2k (O_2K) system (Oroboros Instruments, Innsbruck, Austria) was used to assess mitochondrial respiratory function, as previously described (19, 25). Oxygen flux (JO_2) was measured using an assay that uses a creatine kinase energetic clamp that facilitates measures of JO_2 across a range of ATP-free energy states from near resting to maximum contractions (mimicking a stress test). Mitochondria were energized by additions of 10 mM pyruvate, 2 mM malate, and 2.5 mM octanoylcarnitine. The integrity of the outer mitochondrial membrane was assessed by the addition of cytochrome *c* (5 μM), and samples that exhibited a >25% increase in JO_2 were excluded from analysis. The slope of the relationship between JO_2 and the extramitochondrial free energy for ATP hydrolysis (ΔG_{ATP}), termed oxidative phosphorylation (OXPHOS) conductance, was also calculated. Mitochondrial H_2O_2 production was measured using identical substrate conditions as performed in the Oroboros O_2K Oxygraph via the Amplex ultra red/horseradish peroxidase detection system as previously described (13, 26). Fluorescence spectroscopy was performed using a Quantmaster-400 (Horiba Instruments) with excitation = 565 nm and emission = 590 nm. Fluorescence values were converted to pmoles of H_2O_2 using a standard curve. An estimation of electron leak was calculated by dividing H_2O_2 flux by JO_2 under each identical substrate condition.

Assessment of Oxidized and Reduced Glutathione

Levels of oxidized glutathione (GSSG) and reduced glutathione (GSH) were measured in the distal quadriceps muscles of the AVF limb using ion-paired reverse-phase high-performance liquid chromatography at the Geroscience Redox Biology Core within the Oklahoma Nathan Shock Center on Aging (https://oklahomanathanshockcenteronaging.org/geroscience-redox-biology-core-services/) as previously described (27, 28).

Statistical Analysis

Data are presented as means ± SD. Normality of data was tested with the Shapiro–Wilk test in the visual inspection of QQ plots. Comparisons of data without repeated measurements were performed using two-way ANOVA, and data with repeated measurements were performed using mixed-effects analysis. Šidák's post hoc test was performed for multiple comparisons when significant interactions were detected. All statistical analysis was performed in GraphPad Prism (v.9.0). In all cases, $P < 0.05$ was considered statistically significant.

RESULTS

All data presented in this work are publicly available at https://doi.org/10.6084/m9.figshare.23523216. Figure 1*A* shows a graphical overview and the experimental timeline used in this study. As expected, blood urea nitrogen levels, assessed before the AVF creation, were higher in both male and female mice fed the 0.2% adenine diet compared with animals fed the casein-supplemented control diet (the dashed line in Fig. 1*B* represents the average value of plasma blood urea nitrogen from control mice used in our previous study) (29). Notably, systemic NAC treatment beginning 3 days before AVF surgery did not acutely impact blood urea nitrogen levels (treatment effect, $P = 0.5708$; Fig. 1*B*). The hemodynamic changes captured in the infrarenal aorta and

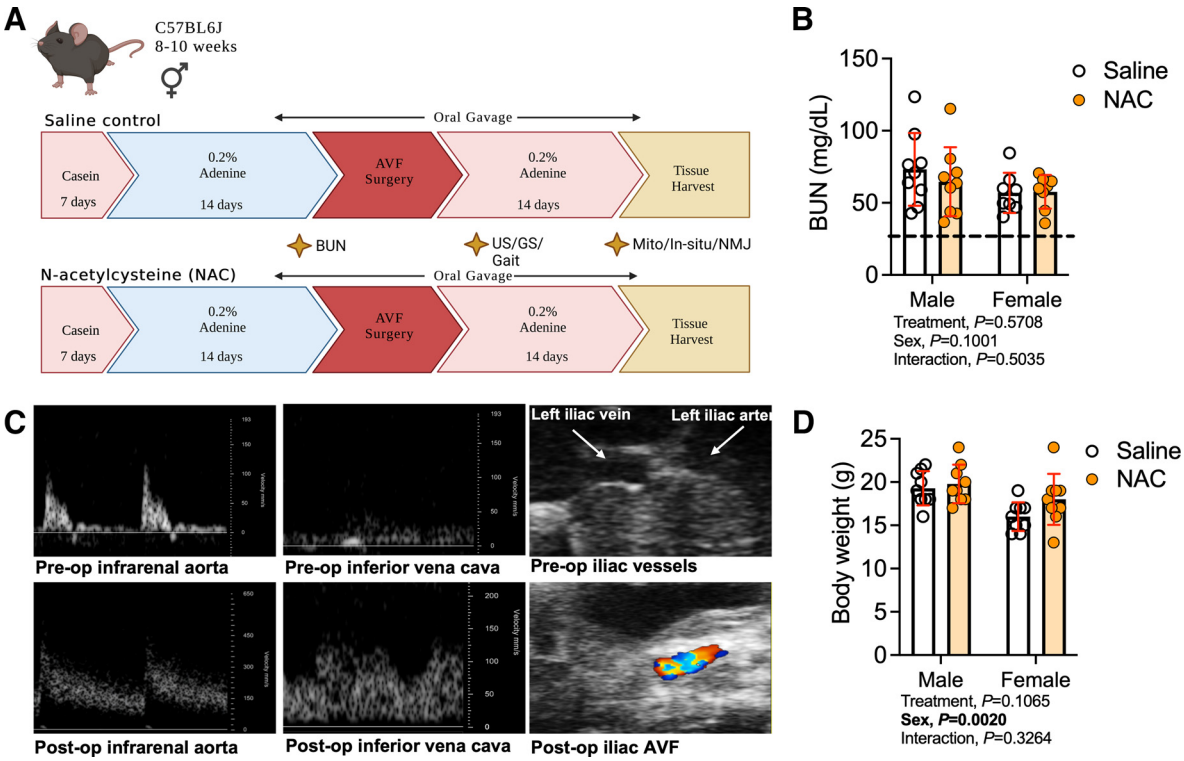

Figure 1. Experimental overview and verification of a mouse model of hemodialysis access-related hand dysfunction. *A*: overall study design. *B*: blood urea nitrogen (BUN) level following 2 wk of 0.2% adenine-supplemented diet ($n = 9$ males/group and $n = 8$ females/group). The dashed line represents the average value of BUN from animals without chronic kidney disease. *C*: Doppler ultrasound (US) images of the infrarenal aorta, inferior vena cava, and left iliac arteriovenous vasculature captured using B-mode prior to the arteriovenous fistula (AVF) surgery and at *postoperative day 13*. *D*: body mass measured at 14 days after the AVF surgery ($n = 9$/sex/group). Data were analyzed using two-way ANOVA with Šidák's post hoc testing. Values are represented as means ± SD. GS, grip strength; NAC, *N*-acetylcysteine; NMJ, neuromuscular junction.

inferior vena cava before the AVF surgery and on *postoperative day 13* provide the unique indirect evidence of the fistula patency as we have previously reported (18, 19, 22). Compared with the preoperative hemodynamic features, animals that underwent AVF surgery exhibited the expected loss of triphasic waveform morphology and associated significantly elevated peak systolic and end-diastolic velocity (~6-fold) profiles in the infrarenal aorta (Fig. 1*C*). Concurrently, an arterialized pulsatile pattern of blood flow as well as greater peak systolic velocity (~4- to 6-fold) relative to preoperative measurements were observed in the inferior vena cava at *postoperative day 13*. Body weight on the day of euthanasia was not impacted by NAC treatment (Fig. 1*D*). Following AVF surgery, mice lost 1–2 g of body weight during the 14 days of postoperative recovery regardless of treatment condition, which is in line with our previous studies (18, 19), demonstrating that the daily oral gavage treatment did not exacerbate the postsurgical weight loss.

NAC Treatment Does Not Alter Vascular Hemodynamics or Muscle Capillary Density Following AVF Surgery

Previous work involving iliac AVF creation in mice has demonstrated clear alterations in the central hemodynamics caused by the sudden decrease in peripheral resistance created by the anastomosis as well as moderate decreases in blood flow to the distal hindlimb (18, 19). Considering that the treatments described herein were provided orally, we first examined if NAC treatment had an impact on hemodynamic alterations, limb perfusion recovery, or muscle capillarization following AVF surgery. In both male and female mice, a significant main effect of time was detected in peak systolic velocities in both the infrarenal aorta and infrarenal vena cava ($P < 0.0001$ for both vessels), confirming the expected hemodynamic adaptations to an AVF (Fig. 2*A*). Regardless of biological sex, NAC treatment had no significant impact on aortic or infrarenal vena cava peak systolic velocities. Consistent with our previous studies using this model, AVF creation significantly reduced blood flow to the TA muscle (~25%) and ventral paw (~75%) immediately following the operation. Local blood flow recovery patterns were dissimilar between measurement locations (Fig. 2*B*). Blood flow recovery to the TA muscle reached ~85% of the nonsurgical limb by *postoperative day 3* and was higher than the nonsurgical limb by *postoperative day 13* (~115%). Peripheral hyperemia within the TA muscle at *postoperative day 13* might be explained in part by skin collateral vessel growth that was clearly evident upon visual inspection and has been previously reported in other murine AVF models (30). In contrast to the TA muscle, blood flow of the ventral paw at *postoperative day 3* was ~50% of the nonsurgical limb and did not fully recover by *postoperative day 13* (~60% of the nonsurgical limb). Like central hemodynamic alterations, NAC treatment did not impact peripheral blood flow recovery in either male or female mice (Fig. 2*B*). Interestingly, there

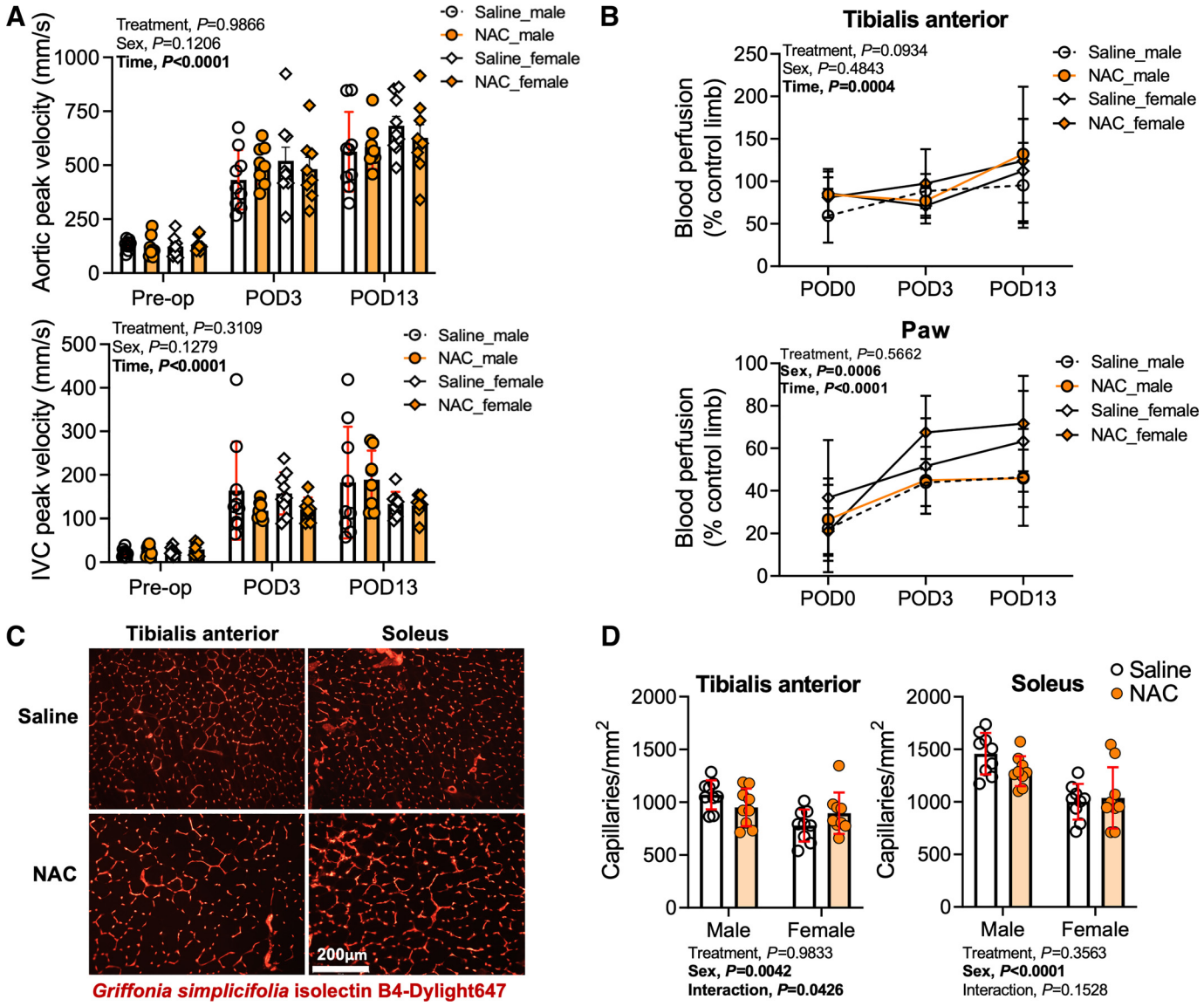

Figure 2. Impact of *N*-acetylcysteine (NAC) treatment on central and peripheral hemodynamics and hindlimb muscle capillarization following arteriovenous fistula (AVF) surgery. *A*: Doppler ultrasound determination of systemic hemodynamics captured at the infrarenal aorta and inferior vena cava (IVC) prior to and at *postoperative day* (*POD*)*3* and *POD13* ($n = 9$ saline-treated males and females and $n = 8$ NAC-treated males and females). *B*: hindlimb blood perfusion to the tibialis anterior muscle and ventral paw immediately after and at *POD3* and *POD13* ($n = 9$ saline-treated males and females and NAC-treated males and $n = 8$ NAC-treated females). *C*: representative images of muscle labeled with *Griffonia simplicifolia* isolectin. Images are from female mice. *D*: capillary density of the tibialis anterior and soleus muscles harvested at *POD14* ($n = 9$/group). Data in *A* and *B* were analyzed using mixed-effects analysis. Data in *D* were analyzed using two-way ANOVA with Šidák's post hoc testing. Values are represented as means ± SD.

was a main effect of sex on paw blood perfusion recovery ($P = 0.0006$). However, post hoc testing did not reveal significant sex differences in either saline- or NAC-treated mice, despite the ~21% difference between male and female mice at *postoperative day 13* (Fig. 2*B*). Next, we measured capillary density within the TA and soleus muscles harvested 14 days after AVF surgery (Fig. 2*D*). Similar to hindlimb perfusion, a main effect for NAC treatment on capillary density was not observed. Interestingly, capillary density was significantly lower in female mice compared with male mice in both the TA ($P = 0.0042$) and soleus ($P < 0.0001$) muscles. These findings suggest that future studies should explore how iliac AVF placement may impact vascular tone in male and female mice.

Impact of NAC Treatment on Hindlimb Muscle Mass and Function Following AVF Surgery

Next, we investigated the impact of NAC treatment on hindlimb neuromotor function and muscle histopathology. Statistically significant main effects for treatment were observed for the muscle masses of both the TA ($P = 0.0120$) and soleus ($P = 0.0452$) muscles. These findings indicate that NAC-treated mice had larger TA (~17%) and soleus (~20%) muscle masses compared with saline-treated control mice that received AVF surgery (Fig. 3*A*). However, the mass of the EDL muscle was only ~6% larger in NAC-treated mice, which was not significantly different from saline-treated mice. To further characterize changes in muscle pathology,

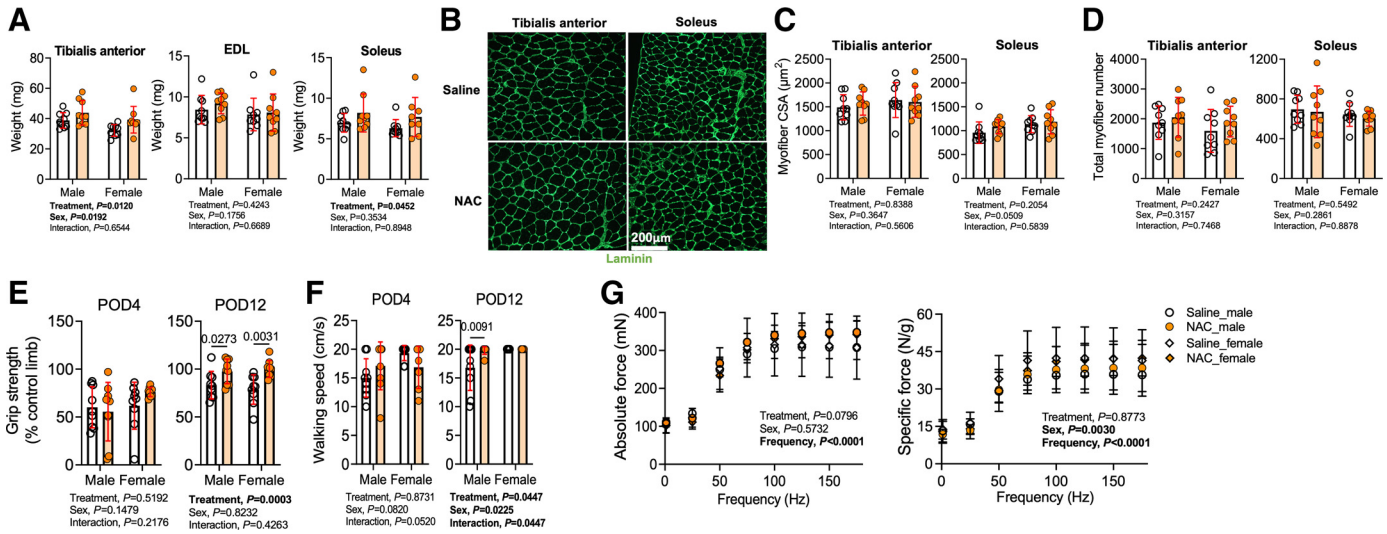

Figure 3. Impact of *N*-acetylcysteine (NAC) treatment on hindlimb skeletal muscle mass and neuromotor function following arteriovenous fistula (AVF) surgery. *A*: muscle mass of the tibialis anterior ($n = 9$/group), extensor digitorum longus (EDL; $n = 9$/group), and soleus ($n = 9$ saline-treated males and females and NAC-treated males and $n = 8$ NAC-treated females) muscles. *B*: representative images of muscle immunolabeled with laminin. Images are from female mice. *C*: mean myofiber cross-sectional area (CSA) in the tibialis anterior and soleus muscles ($n = 9$/group). *D*: total myofiber counts in the tibialis anterior and soleus muscles ($n = 9$/group). *E*: percent recovery of left hindlimb grip strength compared with the contralateral limb at *postoperative day* (*POD*)*4* and *POD12* ($n = 9$/group). *F*: gait speed performed during the treadmill incremental test at *POD4* and *POD12* ($n = 9$/saline-treated group and $n = 7$/NAC-treated group). *G*: in situ muscle contractile function of the EDL muscle at *POD14* ($n = 7$ saline-treated males, $n = 8$ NAC-treated males, $n = 9$ saline-treated females, and $n = 4$ NAC-treated females). Data in *A*–*F* were analyzed using two-way ANOVA with Šidák's post hoc testing. Data in *G* were analyzed using mixed-effects analysis. Values are represented as means ± SD.

immunolabeling of the myofiber membrane with laminin revealed that NAC treatment did not significantly impact mean myofiber CSA (Fig. 3, *B* and *C*) or total myofiber number within these muscles (Fig. 3*D*).

Regarding neuromotor function, grip strength was reduced by 30–40% in the AVF limb at *postoperative day 4* compared with the nonsurgical limb. At *postoperative day 4*, hindlimb grip strength was not different between NAC- and saline-treated mice (Fig. 3*E*). However, at *postoperative day 12*, a significant main effect of NAC treatment was detected ($P = 0.0003$; Fig. 3*E*). Post hoc analysis revealed that both male ($P = 0.0273$) and female ($P = 0.0031$) NAC-treated mice had higher grip strength than saline-treated mice. Like grip strength, walking speed was not affected by NAC treatment at *postoperative day 4* (Fig. 3*F*), but there was a significant main effect for NAC treatment at *postoperative day 12* ($P = 0.0447$). Post hoc testing of *postoperative day 12* walking speeds revealed a significant improvement in male NAC-treated mice ($P = 0.0091$; Fig. 3*F*). In addition to behavioral tests for hindlimb neuromotor function, we also performed rigorous analyses of isometric muscle contractile function using nerve-mediated stimulation to activate all motor units within the EDL muscle. Force-frequency experiments revealed that NAC treatment had no significant impact on either absolute or specific (normalized to muscle mass) forces of the EDL muscle (Fig. 3*G*).

NAC Treatment Promotes Remodeling of the Postsynaptic Neuromuscular Junction

We also explored whether NAC treatment may have affected the morphology of the postsynaptic neuromuscular junction. AchR clusters located on the myofiber membrane were labeled with fluorescently tagged α-bungarotoxin, and high-resolution images were acquired with confocal microscopy. Interestingly, a significant treatment effect was detected for the AChR area ($P = 0.0263$; Fig. 4, *A* and *B*), total endplate area ($P = 0.0240$; Fig. 4, *A* and *E*), and endplate perimeter ($P = 0.0397$; Fig. 4, *A* and *F*), indicating that NAC treatment increased the area of the postsynaptic motor endplate. Post hoc comparisons demonstrated that the AChR area was significantly larger in female NAC-treated mice compared with saline-treated controls ($P = 0.0483$). Interestingly, female mice displayed significantly lower fragmentation of the postsynaptic neuromuscular junction compared with male mice following AVF surgery (Fig. 4*G*).

NAC Treatment Significantly Improves Skeletal Muscle Mitochondrial Function Following AVF Surgery in Female Mice

Recent work from our group has established that mitochondrial respiration rates are negatively impacted by iliac AVF creation (19) and that mitochondria may be a common site for the coalescence of CKD pathologies and hemodynamic disturbances (31). For this reason, we examined whether NAC treatment could improve mitochondrial OXPHOS or reduce mitochondrial ROS levels following AVF creation. Using a recently developed mitochondrial "stress test" (32), NAC treatment was found to have a beneficial main effect on mitochondrial respiration rates ($P = 0.0319$), but a significant treatment × sex interaction revealed that this effect was driven by female mice ($P = 0.0063$; Fig. 5*A*). However, post hoc testing did not establish a difference in oxygen consumption (J_{O_2}) in the female NAC-treated group compared with the saline-treated group (Fig. 5*A*). Analysis of the slope of the relationship between J_{O_2} and energy demand (ΔG_{ATP}), termed OXPHOS conductance, revealed a trending improvement in mitochondrial energy transduction in female NAC-treated mice

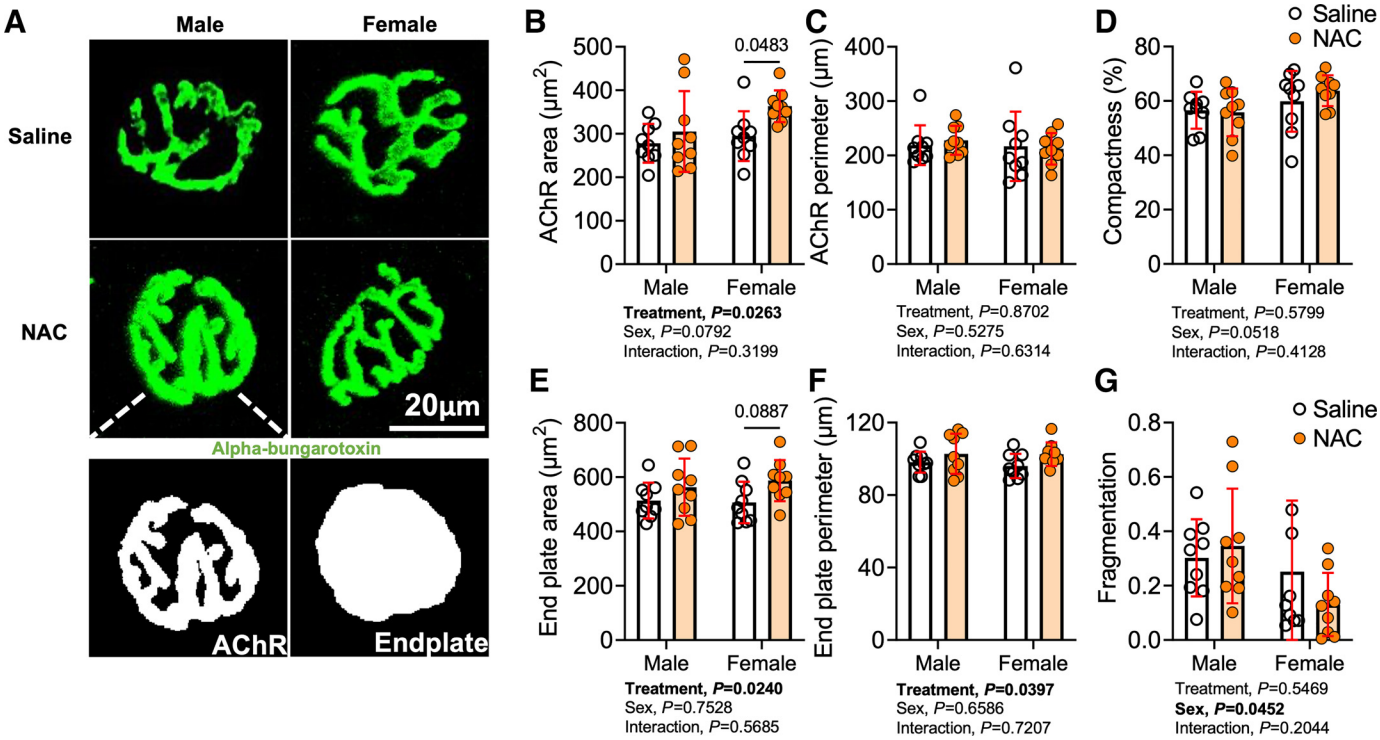

Figure 4. Impact of *N*-acetylcysteine (NAC) treatment on postsynaptic acetylcholine receptor (AChR) clusters. *A*: images of postsynaptic AChRs and motor endplates in male and female. *B* and *C*: area (*B*) and perimeter (*C*) of postsynaptic AChRs. *D*: AChR compactness (AChR compactness (AChR area/endplate area × 100). *E* and *F*: area (*E*) and perimeter (*F*) of motor endplates. *G*: fragmentation (1 − 1/number of AChR clusters). Data were analyzed using two-way ANOVA with Šidák's post hoc testing. Values are represented as means ± SD; $n = 9$/group/sex.

compared with their saline-treated counterparts ($P = 0.0973$; Fig. 5*B*). Using identical substrate conditions, parallel experiments measuring mitochondrial H_2O_2 production were performed. NAC treatment had no significant impact on mitochondrial H_2O_2 production regardless of biological sex or NAC treatment under conditions of energy demand (Fig. 5*C*) or without energy demand (*state 4*; Fig. 5*D*). The estimated mitochondrial electron leak, calculated as H_2O_2 flux/JO_2, was lower in female mice but was unaffected by NAC treatment under conditions of physiologically relevant energy demand ($P = 0.0762$; Fig. 5*E*) or in the absence of energy demand (*state 4*; Fig. 5*F*).

NAC Treatment Had a Minimal Effect on Muscle Redox Status Following AVF Surgery

Considering that NAC can be hydrolyzed into cysteine and serve as a precursor to GSH, we performed measurements of the glutathione redox couple in muscle lysates from the AVF limb. In this regard, NAC treatment increased GSH levels by ~60% in female mice (Fig. 6*A*), although this was not statistically significant, whereas NAC treatment had no effect on GSH levels in male mice. Interestingly, NAC-treated female mice also displayed a nonsignificant increase in GSSG levels (Fig. 6*B*) and, thus, the GSH-to-GSSG ratio was not different in either sex between the treatment groups (Fig. 6*C*).

DISCUSSION

The present study was designed to investigate the therapeutic impact of NAC treatment on access-related limb dysfunction in a recently developed murine iliac AVF model. NAC treatment was explored based on several notable observations in the literature. First, the CKD/ESKD milieu has been shown to promote conditions of chronic oxidative stress, which has also been linked mechanistically to muscle atrophy and weakness (7–9, 12, 33–38). Second, NAC treatment has been previously shown to attenuate muscle fatigue (39–41) and is well tolerated by humans (41). Further to this, NAC can preserve muscle function during hypoxia (42), promote muscle recovery from free radical-induced injury (43), and attenuate motor neuron degeneration (44). Thus, we hypothesized that NAC treatment would diminish AVF-induced limb dysfunction and, if successful, could be easily translated into the clinic for human trials.

In the present study, NAC was found to have several beneficial effects, albeit of modest size, on the AVF limb, including increased muscle mass, improved surgical limb grip strength, greater walking speed, and preservation of the postsynaptic motor endplate area. Although this is the first interventional study in a preclinical AVF model that facilitates assessments of access-related limb dysfunction, there are other preclinical models that confer hemodynamic alterations where NAC has also been found to have a benefit. For example, in a murine model of critical limb ischemia, Lejay et al. (45) found that NAC treatment reduced ischemic tissue damage and improved muscle mitochondrial respiration compared with placebo control treatment. The same group reported similar findings when NAC treatment was provided to apolipoprotein E-deficient mice with critical limb ischemia (46). Moreover, it has been suggested that NAC treatment

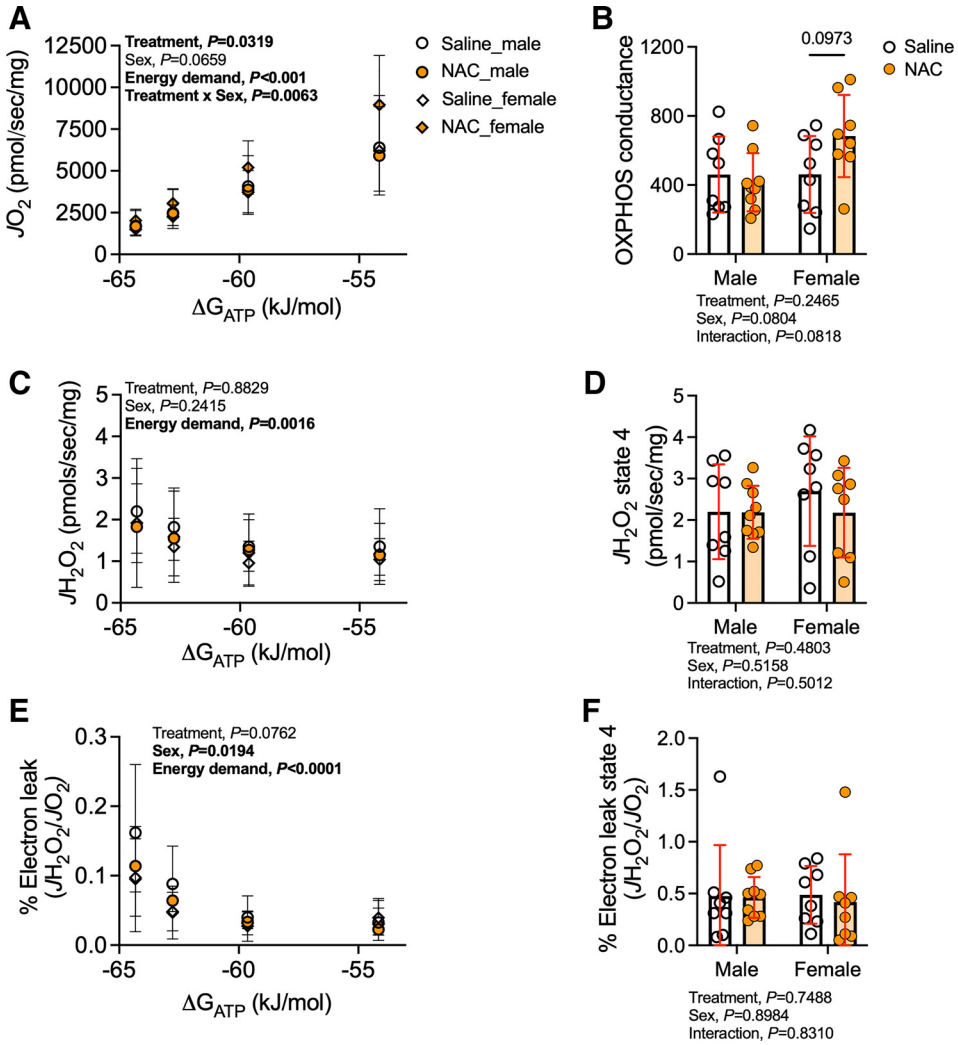

Figure 5. Impact of *N*-acetylcysteine (NAC) treatment on hindlimb skeletal muscle mitochondrial function following arteriovenous fistula (AVF) surgery. *A*: rate of oxygen consumption (JO_2) of plantaris and gastrocnemius mitochondria measured at various energy demands mimicking the stress test from the near-resting condition to maximum contractions in male and female mice. *B*: conductance of oxidative phosphorylation (OXPHOS). *C*: rate of H_2O_2 production (JH_2O_2) determined with identical substrate conditions as performed during the JO_2 measurement in male and female mice. *D*: H_2O_2 production rate at *state 4* after substrate supplementation with pyruvate, malate, and octanoylcarnitine. *E*: electron leak (JH_2O_2/JO_2) was not involved in oxidative phosphorylation in male and female mice. *F*: fraction of electron slips at *state 4* following substrate supplementation with pyruvate, malate, and octanoylcarnitine. Data in *A*, *C*, and *E* were analyzed using a mixed-effects analysis. Data in *B*, *D*, and *F* were analyzed using two-way ANOVA with Šidák's post hoc testing. Values are represented as means ± SD; $n = 8$ saline-treated males and females and NAC-treated females and $n = 9$ NAC-treated males.

may attenuate muscle injury following acute ischemia-reperfusion injury (47).

Interestingly, some of the beneficial effects of NAC treatment following AVF surgery were found to be dependent on the biological sex of the animal. For example, females treated with NAC were the major driver of the main effect of NAC treatment on muscle mitochondrial function, as males treated with NAC had no difference in respiration rates or OXPHOS conductance. The exact mechanisms driving the observed sex-dependent treatment effects are unknown currently and required extensive mechanistic experiments involving manipulation of both sex hormones and chromosomes to rigorously elucidate. Nonetheless, sex differences in NAC treatment have been previously reported in rodent models of central nervous system disorders (48, 49). Potential mechanisms contributing to the observed sex differences in NAC treatment effects in the AVF limb may be related to differences in glutathione metabolism, which have been commonly reported in the literature (50). In this regard, our data are supportive of this hypothesis as NAC treatment

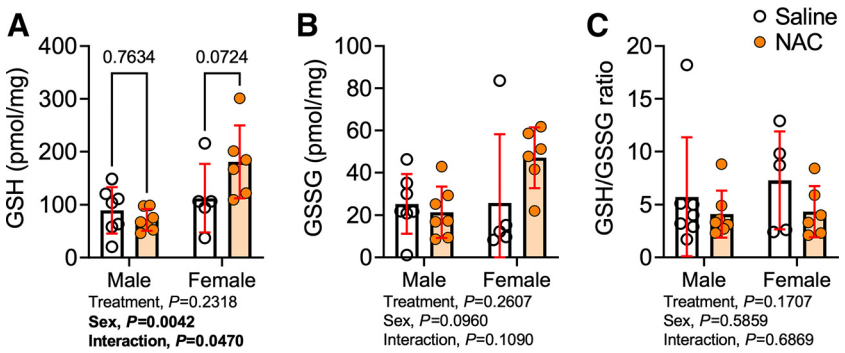

Figure 6. Impact of *N*-acetylcysteine (NAC) treatment on hindlimb muscle redox status following arteriovenous fistula (AVF) surgery. *A*: glutathione level of the quadriceps muscle harvested at *postoperative day 14*. *B*: glutathione disulfide level of the quadriceps muscle harvested at *postoperative day 14*. *C*: ratio of reduced glutathione (GSH) and oxidized glutathione (GSSG). Data were analyzed using two-way ANOVA and Šidák's post hoc testing. Values are represented as means ± SD; $n = 7$ saline- and NAC-treated males, $n = 5$ saline-treated females, and $n = 6$ NAC-treated females).

did not change glutathione levels in male mice but had trending increases in female mice (Fig. 6). The clinical implications of sex-dependent responses to potential antioxidant therapies designed to mitigate ARHD are underscored by the fact that female and male patients have been reported to have different vulnerability to the development of limb- and hand-related symptoms after AVF surgery (51, 52).

Unfortunately, a comprehensive understanding of the mechanisms that drive ARHD in patients with ESKD that undergo AVF creation remains ill defined. To our knowledge, no clinical studies to date have thoroughly examined the neuromuscular alterations that occur in the hand/forearm post-AVF creation in patients with ESKD. This is an important knowledge gap in the field since ARHD presents on a spectrum and even subtle to moderate changes in neuromotor hand function can impact activities of daily living and quality of life (53). Notwithstanding these shortcomings, it is clear that AVF placement will commonly alter hemodynamics in the hand/arm, but access-related hand ischemia resulting in severe clinical symptoms occurs infrequently and only a small percentage of AVF procedures (~5–10%) require surgical remediation ischemia (54). This variation in the clinical presentation and maladaptive responses to AVF-induced hemodynamic perturbations is likely linked to the different compensatory mechanisms that intersect with the preexisting biological factors impacting muscle and neuromotor endplate function. Moreover, previous studies have also reported that reductions in grip strength following AVF surgery are relatively independent of the observed hemodynamic changes (2, 55). In the present study, NAC treatment significantly improved grip strength of the AVF limb but was ineffective at improving the maximal force of the EDL muscle. This discrepancy may be explained by key experimental differences in these outcome variables. For example, grip strength testing is considered a behavioral test, and thus motivation of the animal can impact the voluntary activation of muscles involved in grip strength and thereby impact results. Nonetheless, we used a consistent methodological approach for measuring grip strength in attempts to minimize issues related to motivation (i.e., same animal handler, consistent timing and pressure while pulling mice back from the grip meter, and familiarization sessions). In contrast to grip strength, the in situ muscle function measures involved supramaximal voltage of the proximal motor neuron, ensuring that all motor units were activated. Considering the subtle alterations in postsynaptic neuromuscular junction morphology, it is possible that these effects do not confer a functional impact when supramaximal stimulation is provided. Despite the limitations of these measures, the observations from this preclinical iliac AVF model, as well as the clinical literature, implicate the probability that neuromotor impairment following AVF surgery may be driven by intrinsic neuromuscular pathology.

There are a few limitations of the present study design worthy of discussion. First, CKD mice in this study were not subjected to hemodialysis treatments following creation of the AVF. In contrast to this, it is relatively common that patients with ESKD will undergo catheter-based hemodialysis post-AVF surgery while the AVF matures before being used as the primary vascular access. Second, the experimental design was relatively short in this study, with terminal experiments of limb function being performed 2 wk after AVF creation. In contrast, patients with ESKD undergoing autogenous AVF placement are typically allowed to mature for at least 6 wk and often longer before being used for dialysis access. Thus, much of the clinical information regarding ARHD has been developed using hemodynamic and functional testing of hand function across a longer postoperative period. Finally, patients with ESKD often present with many more comorbid conditions (e.g., diabetes, hypertension, hyperlipidemia, etc.), which have known pathological impacts on the neuromuscular system that were not present in mice fed the adenine diet in the present study.

In summary, systemic NAC treatment improved hindlimb muscle size and paw grip strength following AVF surgery in mice with CKD. Some sex differences were observed in the efficacy of NAC treatment, which are intriguing considering that male and female patients with ESKD have differing susceptibility to ARHD. However, improvements in the postsynaptic motor endplate were also observed in NAC-treated mice that received an AVF, regardless of biological sex. This study establishes the murine iliac AVF model as an important preclinical platform for testing novel therapeutics that have potential to reduce ARHD.

DATA AVAILABILITY

All data presented in this work are publicly available at https://doi.org/10.6084/m9.figshare.23523216.

ACKNOWLEDGMENTS

We acknowledge the Geroscience Redox Biology Core in the Oklahoma Nathan Shock Center for Excellence in the Biology of Aging (5P30AG050911-08) for assistance with analysis of glutathione levels.

GRANTS

This work was supported by National Heart, Lung, and Blood Institute Grant R01HL148597 (to S.T.S.). K.K. was supported by a postdoctoral fellowship from the American Heart Association under Grant POST903198.

DISCLOSURES

No conflicts of interest, financial or otherwise, are declared by the authors.

AUTHOR CONTRIBUTIONS

K.K., E.M.A., S.A.B., T.E.R., and S.T.S. conceived and designed research; K.K., T.A.C., E.M.K., J.M., V.R.P., G.D., E.M.A., B.F., and K.A.O. performed experiments; K.K., T.A.C., E.M.K., J.M., V.R.P., G.D., C.N.M., E.M.A. and B.F. analyzed data; K.K., E.M.A., B.F., S.A.B., T.E.R., and S.T.S. interpreted results of experiments; K.K., T.E.R., and S.T.S. prepared figures; K.K., T.E.R., and S.T.S. drafted manuscript; K.K., T.A.C., E.M.K., J.M., V.R.P., G.D., C.N.M., E.M.A., B.F. K.A.O., S.T.R., S.A.B., T.E.R., and S.T.S. edited and revised manuscript; K.K., T.A.C., E.M.K., J.M., V.R.P., G.D., C.N.M., E.M.A., B.F., K.A.O., S.T.R., S.A.B., T.E.R., and S.T.S. approved final version of manuscript.

REFERENCES

1. **Agarwal AK**, **Haddad NJ**, **Vachharajani TJ**, **Asif A.** Innovations in vascular access for hemodialysis. *Kidney Int* 95: 1053–1063, 2019. doi:10.1016/j.kint.2018.11.046.
2. **Rehfuss JP**, **Berceli SA**, **Barbey SM**, **He Y**, **Kubilis PS**, **Beck AW**, **Huber TS**, **Scali ST.** The spectrum of hand dysfunction after hemodialysis fistula placement. *Kidney Int Rep* 2: 332–341, 2017. doi:10.1016/j.ekir.2016.11.006.
3. **Wang XH**, **Mitch WE**, **Price SR.** Pathophysiological mechanisms leading to muscle loss in chronic kidney disease. *Nat Rev Nephrol* 18: 138–152, 2022. doi:10.1038/s41581-021-00498-0.
4. **Chalupsky M**, **Goodson DA**, **Gamboa JL**, **Roshanravan B.** New insights into muscle function in chronic kidney disease and metabolic acidosis. *Curr Opin Nephrol Hypertens* 30: 369–376, 2021. doi:10.1097/MNH.0000000000000700.
5. **Gamboa JL**, **Roshanravan B**, **Towse T**, **Keller CA**, **Falck AM**, **Yu C**, **Frontera WR**, **Brown NJ**, **Ikizler TA.** Skeletal muscle mitochondrial dysfunction is present in patients with CKD before initiation of maintenance hemodialysis. *Clin J Am Soc Nephrol* 15: 926–936, 2020. doi:10.2215/CJN.10320819.
6. **Thome T**, **Kim K**, **Dong G**, **Ryan TE.** The role of mitochondrial and redox alterations in the skeletal myopathy associated with chronic kidney disease. *Antioxid Redox Signal* 38: 318–337, 2023. doi:10.1089/ars.2022.0143.
7. **Gamboa JL**, **Billings FTt**, **Bojanowski MT**, **Gilliam LA**, **Yu C**, **Roshanravan B**, **Roberts LJ 2nd**, **Himmelfarb J**, **Ikizler TA**, **Brown NJ.** Mitochondrial dysfunction and oxidative stress in patients with chronic kidney disease. *Physiol Rep* 4: e12780, 2016. doi:10.14814/phy2.12780.
8. **Gortan Cappellari G**, **Semolic A**, **Ruozi G**, **Vinci P**, **Guarnieri G**, **Bortolotti F**, **Barbetta D**, **Zanetti M**, **Giacca M**, **Barazzoni R.** Unacylated ghrelin normalizes skeletal muscle oxidative stress and prevents muscle catabolism by enhancing tissue mitophagy in experimental chronic kidney disease. *FASEB J* 31: 5159–5171, 2017. doi:10.1096/fj.201700126R.
9. **Wang D**, **Wei L**, **Yang Y**, **Liu H.** Dietary supplementation with ketoacids protects against CKD-induced oxidative damage and mitochondrial dysfunction in skeletal muscle of 5/6 nephrectomised rats. *Skelet Muscle* 8: 18, 2018. doi:10.1186/s13395-018-0164-z.
10. **Kestenbaum B**, **Gamboa J**, **Liu S**, **Ali AS**, **Shankland E**, **Jue T**, **Giulivi C**, **Smith LR**, **Himmelfarb J**, **de Boer IH**, **Conley K**, **Roshanravan B.** Impaired skeletal muscle mitochondrial bioenergetics and physical performance in chronic kidney disease. *JCI Insight* 5: e133289, 2020. doi:10.1172/jci.insight.133289.
11. **Watson EL**, **Baker LA**, **Wilkinson TJ**, **Gould DW**, **Graham-Brown MPM**, **Major RW**, **Ashford RU**, **Philp A**, **Smith AC.** Reductions in skeletal muscle mitochondrial mass are not restored following exercise training in patients with chronic kidney disease. *FASEB J* 34: 1755–1767, 2020. doi:10.1096/fj.201901936RR.
12. **Kato H**, **Watanabe H**, **Imafuku T**, **Arimura N**, **Fujita I**, **Noguchi I**, **Tanaka S**, **Nakano T**, **Tokumaru K**, **Enoki Y**, **Maeda H**, **Hino S**, **Tanaka M**, **Matsushita K**, **Fukagawa M**, **Maruyama T.** Advanced oxidation protein products contribute to chronic kidney disease-induced muscle atrophy by inducing oxidative stress via CD36/NADPH oxidase pathway. *J Cachexia Sarcopenia Muscle* 12: 1832–1847, 2021. doi:10.1002/jcsm.12786.
13. **Thome T**, **Coleman MD**, **Ryan TE.** Mitochondrial bioenergetic and proteomic phenotyping reveals organ-specific consequences of chronic kidney disease in mice. *Cells* 10: 3282, 2021. doi:10.3390/cells10123282.
14. **Murphy MP**, **Hartley RC.** Mitochondria as a therapeutic target for common pathologies. *Nat Rev Drug Discov* 17: 865–886, 2018. doi:10.1038/nrd.2018.174.
15. **Tietze F.** Enzymic method for quantitative determination of nanogram amounts of total and oxidized glutathione: applications to mammalian blood and other tissues. *Anal Biochem* 27: 502–522, 1969. doi:10.1016/0003-2697(69)90064-5.
16. **Cuadrado A**, **Rojo AI**, **Wells G**, **Hayes JD**, **Cousin SP**, **Rumsey WL**, **Attucks OC**, **Franklin S**, **Levonen AL**, **Kensler TW**, **Dinkova-Kostova AT.** Therapeutic targeting of the NRF2 and KEAP1 partnership in chronic diseases. *Nat Rev Drug Discov* 18: 295–317, 2019. doi:10.1038/s41573-018-0008-x.
17. **Sies H**, **Jones DP.** Reactive oxygen species (ROS) as pleiotropic physiological signalling agents. *Nat Rev Mol Cell Biol* 21: 363–383, 2020. doi:10.1038/s41580-020-0230-3.
18. **Kim K**, **Anderson EM**, **Martin AJ**, **Hu Q**, **Cort TA**, **Harland KC**, **O'Malley KA**, **Lu G**, **Berceli SA**, **Ryan TE**, **Scali ST.** Development of a murine iliac arteriovenous fistula model for examination of hemodialysis access-related limb pathophysiology. *JVS Vasc Sci* 2: 247–259, 2021. doi:10.1016/j.jvssci.2021.09.022.
19. **Anderson EM**, **Kim K**, **Fazzone BJ**, **Harland KC**, **Hu Q**, **Salyers Z**, **Palzkill VR**, **Cort TA**, **Kunz EM**, **Martin AJ**, **Neal D**, **O'Malley KA**, **Berceli SA**, **Ryan TE**, **Scali ST.** Influences of renal insufficiency and ischemia on mitochondrial bioenergetics and limb dysfunction in a novel murine iliac arteriovenous fistula model. *JVS Vasc Sci* 3: 345–362, 2022. doi:10.1016/j.jvssci.2022.10.001.
20. **de Senzi Moraes Pinto R**, **Ferretti R**, **Moraes LH**, **Neto HS**, **Marques MJ**, **Minatel E.** *N*-acetylcysteine treatment reduces TNF-α levels and myonecrosis in diaphragm muscle of mdx mice. *Clin Nutr* 32: 472–475, 2013. doi:10.1016/j.clnu.2012.06.001.
21. **Roseguini BT**, **Silva LM**, **Polotow TG**, **Barros MP**, **Souccar C**, **Han SW.** Effects of *N*-acetylcysteine on skeletal muscle structure and function in a mouse model of peripheral arterial insufficiency. *J Vasc Surg* 61: 777–786, 2015. doi:10.1016/j.jvs.2013.10.098.
22. **Kim K**, **Anderson EM**, **Fazzone BJ**, **O'Malley KA**, **Berceli SA**, **Ryan TE**, **Scali ST.** A murine model of hemodialysis access-related hand dysfunction. *J Vis Exp* 10.3791/63892, 2022. doi:10.3791/63892.
23. **Mayeuf-Louchart A**, **Hardy D**, **Thorel Q**, **Roux P**, **Gueniot L**, **Briand D**, **Mazeraud A**, **Bouglé A**, **Shorte SL**, **Staels B**, **Chrétien F**, **Duez H**, **Danckaert A.** MuscleJ: a high-content analysis method to study skeletal muscle with a new Fiji tool. *Skelet Muscle* 8: 25, 2018. doi:10.1186/s13395-018-0171-0.
24. **Jones RA**, **Reich CD**, **Dissanayake KN**, **Kristmundsdottir F**, **Findlater GS**, **Ribchester RR**, **Simmen MW**, **Gillingwater TH.** NMJ-morph reveals principal components of synaptic morphology influencing structure-function relationships at the neuromuscular junction. *Open Biol* 6: 160240, 2017 [Erratum in *Open Biol* 7: 160335, 2017]. doi:10.1098/rsob.160335.
25. **Thome T**, **Kumar RA**, **Burke SK**, **Khattri RB**, **Salyers ZR**, **Kelley RC**, **Coleman MD**, **Christou DD**, **Hepple RT**, **Scali ST**, **Ferreira LF**, **Ryan TE.** Impaired muscle mitochondrial energetics is associated with uremic metabolite accumulation in chronic kidney disease. *JCI Insight* 6: e139826, 2021. doi:10.1172/jci.insight.139826.
26. **Thome T**, **Salyers ZR**, **Kumar RA**, **Hahn D**, **Berru FN**, **Ferreira LF**, **Scali ST**, **Ryan TE.** Uremic metabolites impair skeletal muscle mitochondrial energetics through disruption of the electron transport system and matrix dehydrogenase activity. *Am J Physiol Cell Physiol* 317: C701–C713, 2019. doi:10.1152/ajpcell.00098.2019.
27. **Puente BN**, **Kimura W**, **Muralidhar SA**, **Moon J**, **Amatruda JF**, **Phelps KL**, **Grinsfelder D**, **Rothermel BA**, **Chen R**, **Garcia JA**, **Santos CX**, **Thet S**, **Mori E**, **Kinter MT**, **Rindler PM**, **Zacchigna S**, **Mukherjee S**, **Chen DJ**, **Mahmoud AI**, **Giacca M**, **Rabinovitch PS**, **Aroumougame A**, **Shah AM**, **Szweda LI**, **Sadek HA.** The oxygen-rich postnatal environment induces cardiomyocyte cell-cycle arrest through DNA damage response. *Cell* 157: 565–579, 2014 [Erratum in *Cell* 157: 1243, 2014]. doi:10.1016/j.cell.2014.03.032.
28. **Rindler PM**, **Cacciola A**, **Kinter M**, **Szweda LI.** Catalase-dependent H_2O_2 consumption by cardiac mitochondria and redox-mediated loss in insulin signaling. *Am J Physiol Heart Circ Physiol* 311: H1091–H1096, 2016. doi:10.1152/ajpheart.00066.2016.
29. **Kim K**, **Anderson EM**, **Thome T**, **Lu G**, **Salyers ZR**, **Cort TA**, **O'Malley KA**, **Scali ST**, **Ryan TE.** Skeletal myopathy in CKD: a comparison of adenine-induced nephropathy and 5/6 nephrectomy models in mice. *Am J Physiol Renal Physiol* 321: F106–F119, 2021. doi:10.1152/ajprenal.00117.2021.
30. **Yamamoto K**, **Protack CD**, **Tsuneki M**, **Hall MR**, **Wong DJ**, **Lu DY**, **Assi R**, **Williams WT**, **Sadaghianloo N**, **Bai H**, **Miyata T**, **Madri JA**, **Dardik A.** The mouse aortocaval fistula recapitulates human arteriovenous fistula maturation. *Am J Physiol Heart Circ Physiol* 305: H1718–H1725, 2013. doi:10.1152/ajpheart.00590.2013.
31. **Berru FN**, **Gray SE**, **Thome T**, **Kumar RA**, **Salyers ZR**, **Coleman M**, **Dennis Le**, **O'Malley K**, **Ferreira LF**, **Berceli SA**, **Scali ST**, **Ryan TE.** Chronic kidney disease exacerbates ischemic limb myopathy in mice via altered mitochondrial energetics. *Sci Rep* 9: 15547, 2019. doi:10.1038/s41598-019-52107-7.

32. **Fisher-Wellman KH**, **Davidson MT**, **Narowski TM**, **Lin CT**, **Koves TR**, **Muoio DM.** Mitochondrial diagnostics: a multiplexed assay platform for comprehensive assessment of mitochondrial energy fluxes. *Cell Rep* 24: 3593–3606.e10, 2018. doi:10.1016/j.celrep.2018.08.091.
33. **Raj DS**, **Dominic EA**, **Pai A**, **Osman F**, **Morgan M**, **Pickett G**, **Shah VO**, **Ferrando A**, **Moseley P.** Skeletal muscle, cytokines, and oxidative stress in end-stage renal disease. *Kidney Int* 68: 2338–2344, 2005. doi:10.1111/j.1523-1755.2005.00695.x.
34. **Beetham KS**, **Howden EJ**, **Small DM**, **Briskey DR**, **Rossi M**, **Isbel N**, **Coombes JS.** Oxidative stress contributes to muscle atrophy in chronic kidney disease patients. *Redox Rep* 20: 126–132, 2015. doi:10.1179/1351000214Y.0000000114.
35. **Avin KG**, **Chen NX**, **Organ JM**, **Zarse C**, **O'Neill K**, **Conway RG**, **Konrad RJ**, **Bacallao RL**, **Allen MR**, **Moe SM.** Skeletal muscle regeneration and oxidative stress are altered in chronic kidney disease. *PLoS One* 11: e0159411, 2016. doi:10.1371/journal.pone.0159411.
36. **Enoki Y**, **Watanabe H**, **Arake R**, **Sugimoto R**, **Imafuku T**, **Tominaga Y**, **Ishima Y**, **Kotani S**, **Nakajima M**, **Tanaka M**, **Matsushita K**, **Fukagawa M**, **Otagiri M**, **Maruyama T.** Indoxyl sulfate potentiates skeletal muscle atrophy by inducing the oxidative stress-mediated expression of myostatin and atrogin-1. *Sci Rep* 6: 32084, 2016. doi:10.1038/srep32084.
37. **Liakopoulos V**, **Roumeliotis S**, **Gorny X**, **Eleftheriadis T**, **Mertens PR.** Oxidative stress in patients undergoing peritoneal dialysis: a current review of the literature. *Oxid Med Cell Longev* 2017: 3494867, 2017. doi:10.1155/2017/3494867.
38. **Wang M**, **Hu R**, **Wang Y**, **Liu L**, **You H**, **Zhang J**, **Wu X**, **Pei T**, **Wang F**, **Lu L**, **Xiao W**, **Wei L.** Atractylenolide III attenuates muscle wasting in chronic kidney disease via the oxidative stress-mediated PI3K/AKT/mTOR pathway. *Oxid Med Cell Longev* 2019: 1875471, 2019. doi:10.1155/2019/1875471.
39. **Diaz PT**, **Brownstein E**, **Clanton TL.** Effects of *N*-acetylcysteine on in vitro diaphragm function are temperature dependent. *J Appl Physiol (1985)* 77: 2434–2439, 1994. doi:10.1152/jappl.1994.77.5.2434.
40. **Khawli FA**, **Reid MB.** *N*-acetylcysteine depresses contractile function and inhibits fatigue of diaphragm in vitro. *J Appl Physiol (1985)* 77: 317–324, 1994. doi:10.1152/jappl.1994.77.1.317.
41. **Reid MB**, **Stokić DS**, **Koch SM**, **Khawli FA**, **Leis AA.** *N*-acetylcysteine inhibits muscle fatigue in humans. *J Clin Invest* 94: 2468–2474, 1994. doi:10.1172/JCI117615.
42. **Mohanraj P**, **Merola AJ**, **Wright VP**, **Clanton TL.** Antioxidants protect rat diaphragmatic muscle function under hypoxic conditions. *J Appl Physiol (1985)* 84: 1960–1966, 1998. doi:10.1152/jappl.1998.84.6.1960.
43. **van der Laan L**, **Oyen WJ**, **Verhofstad AA**, **Tan EC**, **ter Laak HJ**, **Gabreels-Festen A**, **Hendriks T**, **Goris RJ.** Soft tissue repair capacity after oxygen-derived free radical-induced damage in one hindlimb of the rat. *J Surg Res* 72: 60–69, 1997. doi:10.1006/jsre.1997.5167.
44. **Henderson JT**, **Javaheri M**, **Kopko S**, **Roder JC.** Reduction of lower motor neuron degeneration in wobbler mice by *N*-acetyl-L-cysteine. *J Neurosci* 16: 7574–7582, 1996. doi:10.1523/JNEUROSCI.16-23-07574.1996.
45. **Lejay A**, **Paradis S**, **Lambert A**, **Charles AL**, **Talha S**, **Enache I**, **Thaveau F**, **Chakfe N**, **Geny B.** *N*-acetyl cysteine restores limb function, improves mitochondrial respiration, and reduces oxidative stress in a murine model of critical limb ischaemia. *Eur J Vasc Endovasc Surg* 56: 730–738, 2018. doi:10.1016/j.ejvs.2018.07.025.
46. **Lejay A**, **Charles AL**, **Georg I**, **Goupilleau F**, **Delay C**, **Talha S**, **Thaveau F**, **Chakfé N**, **Geny B.** Critical limb ischaemia exacerbates mitochondrial dysfunction in *ApoE*$^{-/-}$ mice compared with *ApoE*$^{+/+}$ mice, but N-acetyl cysteine still confers protection. *Eur J Vasc Endovasc Surg* 58: 576–582, 2019. doi:10.1016/j.ejvs.2019.03.028.
47. **Bolcal C**, **Yildirim V**, **Doganci S**, **Sargin M**, **Aydin A**, **Eken A**, **Ozal E**, **Kuralay E**, **Demirkilic U**, **Tatar H.** Protective effects of antioxidant medications on limb ischemia reperfusion injury. *J Surg Res* 139: 274–279, 2007. doi:10.1016/j.jss.2006.10.043.
48. **Durieux AM**, **Fernandes C**, **Murphy D**, **Labouesse MA**, **Giovanoli S**, **Meyer U**, **Li Q**, **So PW**, **McAlonan G.** Targeting glia with *N*-acetylcysteine modulates brain glutamate and behaviors relevant to neurodevelopmental disorders in C57BL/6J mice. *Front Behav Neurosci* 9: 343, 2015. doi:10.3389/fnbeh.2015.00343.
49. **Monte AS**, **da Silva FER**, **Lima CNC**, **Vasconcelos GS**, **Gomes NS**, **Miyajima F**, **Vasconcelos SMM**, **Gama CS**, **Seeman MV**, **de Lucena DF**, **Macedo DS.** Sex influences in the preventive effects of *N*-acetylcysteine in a two-hit animal model of schizophrenia. *J Psychopharmacol* 34: 125–136, 2020. doi:10.1177/0269881119875979.
50. **Wang L**, **Ahn YJ**, **Asmis R.** Sexual dimorphism in glutathione metabolism and glutathione-dependent responses. *Redox Biol* 31: 101410, 2020. doi:10.1016/j.redox.2019.101410.
51. **Rocha A**, **Silva F**, **Queirós J**, **Malheiro J**, **Cabrita A.** Predictors of steal syndrome in hemodialysis patients. *Hemodial Int* 16: 539–544, 2012. doi:10.1111/j.1542-4758.2012.00684.x.
52. **Leake AE**, **Winger DG**, **Leers SA**, **Gupta N**, **Dillavou ED.** Management and outcomes of dialysis access-associated steal syndrome. *J Vasc Surg* 61: 754–760, 2015. doi:10.1016/j.jvs.2014.10.038.
53. **Sen I**, **Tripathi RK.** Dialysis access-associated steal syndromes. *Semin Vasc Surg* 29: 212–226, 2016. doi:10.1053/j.semvascsurg.2017.04.002.
54. **Huber TS**, **Larive B**, **Imrey PB**, **Radeva MK**, **Kaufman JM**, **Kraiss LW**, **Farber AM**, **Berceli SA**; **HFMS Group.** Access-related hand ischemia and the Hemodialysis Fistula Maturation Study. *J Vasc Surg* 64: 1050–1058.e1, 2016. doi:10.1016/j.jvs.2016.03.449.
55. **Kmentova T**, **Valerianova A**, **Kovarova L**, **Lachmanova J**, **Hladinova Z**, **Malik J.** Decrease of muscle strength in vascular access hand due to silent ischaemia. *J Vasc Access* 19: 573–577, 2018. doi:10.1177/1129729818763287.